9-17-2008

Inverting amplitude and phase to reconstruct tip-sample interaction forces in tapping mode atomic force microscopy

Shuiqing Hu
Purdue University - Main Campus, shuiqing@purdue.edu

Arvind Raman
Birck Nanotechnology Center, Purdue University, raman@purdue.edu

Nanotechnology **19** (2008) 375704 (11pp) doi:10.1088/0957-4484/19/37/375704

Inverting amplitude and phase to reconstruct tip–sample interaction forces in tapping mode atomic force microscopy

Shuiqing Hu and Arvind Raman

School of Mechanical Engineering, Birck Nanotechnology Center, Purdue University, West Lafayette, IN 47907, USA

Received 13 February 2008, in final form 20 May 2008
Published 1 August 2008
Online at stacks.iop.org/Nano/19/375704

Abstract

Quantifying the tip–sample interaction forces in amplitude-modulated atomic force microscopy (AM-AFM) has been an elusive yet important goal in nanoscale imaging, manipulation and spectroscopy using the AFM. In this paper we present a general theory for the reconstruction of tip–sample interaction forces using integral equations for AM-AFM and Chebyshev polynomial expansions. This allows us to reconstruct the tip–sample interactions using standard amplitude and phase versus distance curves acquired in AM-AFM regardless of tip oscillation amplitude and in both the net attractive and repulsive regimes of oscillation. Systematic experiments are performed to reconstruct interaction forces on polymer samples to demonstrate the power of the theoretical approach.

(Some figures in this article are in colour only in the electronic version)

1. Introduction

In dynamic atomic force microscopy (dAFM), the tip–sample interaction forces are not directly measured but rather need to be extracted or reconstructed from measured frequency or amplitude or phase shifts as the oscillating probe is brought closer to the sample surface. Knowledge of these interaction forces reveals valuable information about nanoscale local material properties including chemical composition [1], short and long range forces [2], elasticity [3], plasticity [4] and friction [5]. This remarkable capability to quantitatively measure material properties at the nanoscale has propelled efforts to reconstruct interaction forces in dAFM.

The reconstruction of tip–sample interaction forces has for the most part been the privilege of frequency-modulated AFM (FM-AFM) [6, 7] where a phase-locked loop tracks the nonlinear resonance frequency of the oscillating nanotip as it is brought close to a sample surface. The theoretical basis for the reconstruction tip–sample interaction forces in FM-AFM is the integral equation developed originally by Dürig [8, 9] using Hamilton–Jacobi perturbation theory. This theory applies to the free, undamped oscillations of the AFM probe that are perturbed by the presence of nonlinear tip–sample interaction forces.This integral equation allows the inversion of the measured nonlinear frequency shifts to the tip–sample interaction forces. Dürig implemented the large amplitude assumption or short range interaction force assumption, under which the integral equation becomes the Abel integral equation [10] and can be inverted to reconstruct the interaction forces. This method has become by far the most popular method in FM-AFM force spectroscopy and has been used to chemically identify individual surface atoms [11, 12] and even measure the three-dimensional force fields with atomic resolution [13, 14]. Recently, Sader and Jarvis [15, 16] have modified the integral equation inversion routine to reconstruct general tip–sample interactions without being limited by the large amplitude or short range forces assumption. Dürig [17] theoretically proposed a technique which uses all the amplitudes and phase of higher harmonics through Chebyshev polynomial expansion to reconstruct the tip sample interaction forces. This method is promising for small amplitude operations in which the amplitude is much smaller than the decay length of the interaction forces.

In contrast, the theoretical basis for force reconstruction in AM-AFM or tapping mode AFM is poorly developed. In AM-AFM the drive frequency is constant and the amplitude and phase of oscillation are monitored during approach to the sample. Hölscher [18] developed an integral equation for AM-AFM that allows the inversion of experimentally measured amplitude and phase distance curves into interaction forces.

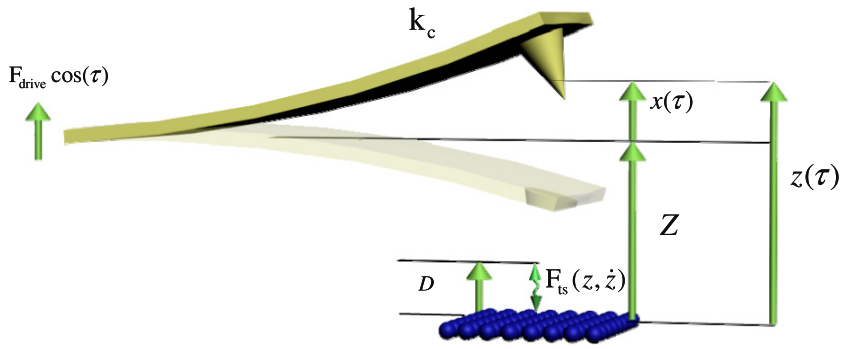

Figure 1. Schematic diagram of the dynamic cantilever configurations with harmonic base excitation $F_{\text{drive}}\cos(\tau)$.

However in [18] it is also assumed that the tip amplitude is large relative to the decay length of the tip–sample interaction forces allowing the inversion of Abel's integral equation; as a result the theory is not general enough to include applications with long range interaction forces. Moreover, jumps can occur in the amplitude and phase versus distance curves in AM-AFM and thus in Hölscher's approach the data points after the jump cannot be used for a reliable reconstruction of the repulsive interaction forces; only the attractive interaction forces can be reconstructed. Sugawara *et al* [19] suggested overcoming this jump problem with the phase-modulation method. In this technique, the phase difference between the excitation and the oscillation of the microcantilever is used as the feedback signal, and the amplitude is kept constant by an additional feedback which is added to the electronics of a conventional AM-AFM. Hölscher [20] demonstrated that the phase-modulation technique is capable of measuring tip–sample forces without any jumps caused by instabilities. However, this technique needs significant hardware electronics modification to the conventional AM-AFM. Recently, Lee and Jhe [21] proposed a general theoretical method to reconstruct interaction forces in AM-AFM using Laplace transform and modified Bessel functions. However, a systematic reconstruction of interaction forces from the experimental measured amplitude and phase distance curves has not been performed.

In this paper, we derive integral equations of AM-AFM with fewer restrictions on the nonconservative forces than in Lee and Jhe [21], and solve it using the Chebyshev polynomial expansion method that ensures excellent convergence of the reconstruction. This theoretical approach allows the use of standard amplitude and phase distance curves to reconstruct interaction forces in both the attractive and repulsive regimes, regardless of tip oscillation amplitude. Moreover the theory can be used to predict the peak interaction forces directly from amplitude and phase distance curves, thus allowing the direct measurement of imaging forces exerted on the sample without the need for specialized cantilevers or signal processing methods. Because the method uses Chebyshev polynomial expansions, it can be easily included as a MATLAB routine in commercial AFM systems allowing experimentalists to deduce interaction forces from experimental amplitude and phase distance curves. We illustrate the method using numerical simulations and detailed experiments on polymer samples under ambient conditions.

2. An integral equation for AM-AFM

Based on a one-mode discretization of the continuous dynamic cantilever model [22], the tip motion in a specific microcantilever eigenmode can be approximately described by an equivalent point mass model [23] after scaling natural time t by the driving frequency $\omega(\tau = \omega t)$,

$$\Omega^2\frac{\mathrm{d}^2x}{\mathrm{d}\tau^2} + \frac{\Omega}{Q}\frac{\mathrm{d}x}{\mathrm{d}\tau} + x = \frac{F_{\text{ts}}(z,\dot{z})}{k_{\text{c}}} + \frac{F_{\text{drive}}\cos(\tau)}{k_{\text{c}}}, \qquad (1)$$

where $x(\tau)$ is the tip motion, and $z(\tau)$ is the instantaneous gap between the nanoscale tip and the sample (see figure 1). Let Z be the cantilever sample separation so that $z(\tau) \approx Z + x(\tau)$. $F_{\text{ts}}(z,\dot{z})$ is the tip sample interaction force that depends on instantaneous gap and tip velocity k_{c} is the equivalent stiffness of the driven mode of the microcantilever [22]. $\Omega = \omega/\omega_0$, where ω_0 is a linear resonance frequency of the cantilever, and Q is the quality factor of the chosen mode of the cantilever. F_{drive} is the magnitude of the driving inertial or magnetic force.

In order to derive an integral equation for AM-AFM, we use the one-term harmonic balance method [24, 25] and substitute the assumed harmonic tip motion $x(\tau) = A\cos(\theta) = A\cos(\tau+\varphi)$ into equation (1)

$$\Omega^2 A\cos(\tau+\varphi) - \frac{\Omega}{Q}A\sin(\tau+\varphi) + A\cos(\tau+\varphi) = \frac{F_{\text{ts}}(z,\dot{z})}{k_{\text{c}}} + \frac{F_{\text{drive}}\cos(\tau)}{k_{\text{c}}}. \qquad (2)$$

Assuming the conservative interaction force as $F_{\text{tsc}}(z) = [F_{\text{ts}}(z,\dot{z}) + F_{\text{ts}}(z,-\dot{z})]/2$ [16], and the nonconservative interaction force as $F_{\text{tsnc}}(z,\dot{z}) = [F_{\text{ts}}(z,\dot{z}) - F_{\text{ts}}(z,-\dot{z})]/2$, we have

$$F_{\text{ts}}(z,\dot{z}) = F_{\text{tsc}}(z) + F_{\text{tsnc}}(z,\dot{z}), \qquad \text{and} \qquad F_{\text{tsnc}}(z,\dot{z}) = -F_{\text{tsnc}}(z,-\dot{z}). \qquad (3)$$

This implies that the nonconservative interactions are an odd function of tip velocity, a key requirement for physically realistic nonconservative interactions such as surface hysteresis, viscoelasticity, and long range hysteresis. Notice that instantaneous gap and its rate are given by $z(\tau) = Z + x(\tau) = Z + A\cos(\theta)$ and $\dot{z}(\tau) = -A\sin(\theta)$ which can be substituted into equation (3) yielding:

$$F_{\text{ts}}(z,\dot{z}) = \bar{F}_{\text{ts}}[Z + A\cos(\theta), -A\sin(\theta)] = \bar{F}_{\text{tsc}}[Z + A\cos(\theta)] + \bar{F}_{\text{tsnc}}[A\cos(\theta), -A\sin(\theta)].$$

Expanding $F_{ts}(z, \dot{z})$ into a Fourier series we have

$$F_{ts}(z, \dot{z}) = \bar{F}_{ts}[Z + A\cos(\theta), -A\sin(\theta)] = F_{ts\,cos}\cos(\theta) + F_{ts\,sin}\sin(\theta) + \text{higher harmonics}, \quad (4)$$

where $F_{ts\,cos}$ and $F_{ts\,sin}$ are the cosine and sine Fourier coefficients. By invoking the antisymmetry with respect to tip velocity of the nonconservative forces $F_{tsnc}(z, \dot{z}) = -F_{tsnc}(z, -\dot{z})$, it can be shown that (see the appendix for details)

$$F_{ts\,cos} = \frac{1}{\pi}\int_0^{2\pi} \bar{F}_{tsc}[Z + A\cos(\theta)]\cos(\theta)\,d\theta,$$
$$F_{ts\,sin} = \frac{1}{\pi}\int_0^{2\pi} \bar{F}_{tsnc}[Z + A\cos(\theta), -A\sin(\theta)]\sin(\theta)\,d\theta. \quad (5)$$

Because the quality factor Q is high in ambient conditions the higher order terms of the Fourier series can be neglected. Following the one-term harmonic balance method or the describing function method [24, 25], we substitute equation (5) into equation (2) and equate the sine and cosine terms on both sides of the equation, to get

$$F_{drive}\sin(\varphi) = -2A\Omega\zeta_e,$$
$$F_{drive}\cos(\varphi) = A\left(\Omega_e^2 - \Omega^2\right), \quad (6)$$

where the effective nonlinear damping factor ζ_e and effective nonlinear frequency Ω_e are

$$\zeta_e = \frac{1}{2Q} + \frac{1}{2\pi A\Omega k_c}\int_0^{2\pi} F_{tsnc}[Z + A\cos(\theta), -A\sin(\theta)]\sin(\theta)\,d\theta, \quad (7)$$

$$\Omega_e^2 = 1 - \frac{1}{\pi A k_c}\int_0^{2\pi} F_{tsc}[Z + A\cos(\theta)]\cos(\theta)\,d\theta. \quad (8)$$

Thus the *conservative and nonconservative interactions can be decoupled* in the sense that F_{tsnc} is only related to the effective nonlinear damping factor ζ_e as shown in equation (7) and F_{tsc} is only related to the nonlinear resonance frequency Ω_e as shown in equation (8). Recalling the amplitude response of the driven probe far from the sample $F_{drive}^2 = A_0^2[\frac{\Omega^2}{Q^2} + (1-\Omega^2)^2]$, where A_0 is the initial amplitude when tip is far away from the sample and defining amplitude setpoint ratio $A_{ratio} = A/A_0$, equation (6) becomes

$$\frac{\sin(\varphi)}{A_{ratio}}\sqrt{\frac{\Omega^2}{Q^2} + (1-\Omega^2)^2} = -2\Omega\zeta_e, \quad (9)$$

$$\frac{\cos(\varphi)}{A_{ratio}}\sqrt{\frac{\Omega^2}{Q^2} + (1-\Omega^2)^2} + \Omega^2 - 1 = \Omega_e^2 - 1. \quad (10)$$

Notice that $\sin(\varphi)/A_{ratio}$ measures the effective nonlinear damping factor ζ_e and $\cos(\varphi)/A_{ratio}$ measures the effective nonlinear resonance frequency Ω_e. Ω_e changes due to conservative nonlinear interactions as shown in equation (8).

Equations (9) and (10) are the general integral equations that can be used to reconstruct the interaction forces. In this article we focus on reconstructing the conservative interaction forces using equation (10). In equation (10) the ratio of drive frequency to resonance frequency Ω, the amplitude ratio A_{ratio}, the quality factor Q and the phase φ are all experimentally measurable quantities. Furthermore, the nonlinear frequency shift $(\Omega_e^2 - 1)$ can be measured from the amplitude and phase versus distance curves using equation (10). Then from the definition of the nonlinear resonance frequency Ω_e given in equation (8), we have

$$-\pi k_c A(\Omega_e^2 - 1) = \int_0^{2\pi} F_{tsc}[Z + A\cos(\theta)]\cos(\theta)\,d\theta. \quad (11)$$

We define the nearest tip sample distance as $D = Z - A$ so that the nearest tip sample distance D is the negative of the indentation δ when tip is in contact with sample. Noting that the instantaneous tip–sample gap $z(\tau) = Z + x(\tau) = Z + A\cos(\theta)$, $\cos(\theta) = (z - D - A)/A$, and $-\sin(\theta)\,d\theta = dz/A$, the integral equation (11) can be transformed to

$$-\frac{\pi k_c A^2}{2}(\Omega_e^2 - 1) = \int_D^{D+2A} F_{tsc}(z)\frac{z - D - A}{\sqrt{A^2 - (z - D - A)^2}}\,dz. \quad (12)$$

Substituting equation (12) into equation (10), we obtain,

$$-\frac{\pi k_c A^2}{2}\left[\Omega^2 - 1 + \frac{\cos(\varphi)}{A_{ratio}}\sqrt{\frac{\Omega^2}{Q^2} + (1-\Omega^2)^2}\right] = \int_D^{D+2A} F_{tsc}(z)\frac{z - D - A}{\sqrt{A^2 - (z - D - A)^2}}\,dz. \quad (13)$$

When the drive frequency equals the linear resonance frequency, $(\Omega = 1)$, we obtain,

$$-\frac{\pi k_c A^2\cos(\varphi)}{2A_{ratio}Q} = \int_D^{D+2A} F_{tsc}(z)\frac{z - D - A}{\sqrt{A^2 - (z - D - A)^2}}\,dz. \quad (14)$$

Every data point in the amplitude and phase distance curves corresponds to one such equation with a specific nearest approach distance D. Solving these integral equations then enables the reconstruction of the conservative tip sample interaction force F_{tsc} as a function of instantaneous gap z.

Our strategy is to expand interaction force F_{tsc} as a series expansion of special functions. If these special functions can be integrated, then we can solve the resulting algebraic matrix equation for the coefficients of the special functions and reconstruct F_{tsc} with these coefficients. Since F_{tsc} is non-periodic and defined in a bounded domain, Chebyshev polynomials of the first kind are expected to be an optimal basis for the reconstruction of the interaction force [26]. Chebyshev polynomials are expected to be an optimal basis sets due to their following properties: (i) ease of computation (ii) completeness, which means that any solution can be represented to an arbitrarily high degree of accuracy by taking N, the truncation, to be sufficiently large and (iii) rapid convergence. In fact, Chebyshev polynomials are so-called 'entire functions' or functions without singularities anywhere in the complex plane except at ∞. Furthermore, they have 'supergeometric' convergence [26] which means that the expansion coefficients versus N, the number of terms in the expansion has a progressively negative slope (rather than a constant slope) on a log-linear graph.

During the measurement of a dynamic amplitude distance curve, the instantaneous gap between the tip and the sample z would vary between $D_{\min}$ and $D_{\max}$, where $D_{\min}$ and $D_{\max}$ correspond to the minimum and maximum value of z in the whole dynamic distance curve. Since the Chebyshev polynomial of the first kind T_n [27] is defined in the domain $[-1, 1]$, so the reconstructed interaction force $F_{\text{tsc}}(z)$ should also be defined in a bounded domain, say $z \in [D_1, D_2]$. In principle, D_1 should be $D_{\min}$, the minimum value for the lower limit of the integral, and D_2 should be $D_{\max} + 2A$, the maximum value of the upper limit of the integral for the entire amplitude or phase distance curve. In practice though the $F_{\text{tsc}} \approx 0$ for a large range of $z < D_{\max} + 2A$. Thus D_2 can be chosen to be $< D_{\max} + 2A$, assuming that $F_{\text{tsc}} \approx 0$ for $z > D_2$. As we will see later this has an added advantage since the convergence of the reconstructed force is faster if performed over a smaller range of z values. Once D_1 and D_2 are decided upon, we can map z to $\hat{z}$, so that $\hat{z} \in [-1, 1]$,

$$\hat{z} = \frac{2z - D_1 - D_2}{D_2 - D_1}. \tag{15}$$

Expanding $F_{\text{tsc}}[\hat{z}]$ as Chebyshev polynomials, we have,

$$F_{\text{tsc}}(\hat{z}) = F_{\text{tsc}}\left[\frac{2z - D_1 - D_2}{D_2 - D_1}\right] = \sum_{n=0}^{\infty} C_n T_n(\hat{z})$$
$$\approx \sum_{n=0}^{N} C_n T_n(\hat{z}) \tag{16}$$

where C_n are the Chebyshev polynomial coefficients, and T_n are Chebyshev polynomials of the first kind. Substituting the expanded F_{tsc} into equation (14), we obtain,

$$-\frac{\pi k_c A^2 \cos(\varphi)}{2A_{\text{ratio}} Q} = \int_D^{D+2A} \sum_{n=0}^{N} C_n T_n(\hat{z}) \frac{z - D - A}{\sqrt{A^2 - (z - D - A)^2}}\, \mathrm{d}z. \tag{17}$$

Switching the order of integration and summation and noticing that $F_{\text{tsc}}(z) \approx 0$ for $z > D_2$, and we obtain

$$\sum_{n=0}^{N} C_n \int_D^{D_2} T_n(\hat{z}) \frac{z - D - A}{\sqrt{A^2 - (z - D - A)^2}}\, \mathrm{d}z \approx -\frac{\pi k_c A^2 \cos(\varphi)}{2A_{\text{ratio}} Q}. \tag{18}$$

Setting $I_n = \int_D^{D_2} T_n(\hat{z}) \frac{z-D-A}{\sqrt{A^2-(z-D-A)^2}}\, \mathrm{d}z$, the final algebraic equation is given as follows,

$$\sum_{n=0}^{N} C_n I_n = -\frac{\pi k_c A^2 \cos(\varphi)}{2A_{\text{ratio}} Q}. \tag{19}$$

Notice that for every nearest tip–sample distance D,[1] there is one such equation. If the measured amplitude and phase distance curves have M points, then we have the following matrix equation

$$\begin{pmatrix} I_0(D_1) & I_1(D_1) & I_2(D_1) & \dots & I_N(D_1) \\ I_0(D_2) & I_1(D_2) & I_2(D_2) & \dots & I_N(D_2) \\ \dots & \dots & \dots & \dots & \dots \\ I_0(D_M) & I_1(D_M) & I_2(D_M) & \dots & I_N(D_M) \end{pmatrix} \begin{pmatrix} C_0 \\ C_1 \\ \dots \\ C_n \end{pmatrix} = \begin{pmatrix} -\frac{\pi k_c A^2 \cos(\varphi(D_1))}{2A_{\text{ratio}} Q} \\ -\frac{\pi k_c A^2 \cos(\varphi(D_2))}{2A_{\text{ratio}} Q} \\ \dots \\ -\frac{\pi k_c A^2 \cos(\varphi(D_M))}{2A_{\text{ratio}} Q} \end{pmatrix}. \tag{20}$$

The matrix in (equation (20)) can be inverted to determine the Chebyshev polynomial coefficients $(C_0, C_1, \dots, C_n)$ using the QR decomposition method in MATLAB. Finally, the reconstructed the interaction force will then be

$$F_{\text{tsc}}(\hat{z}) \approx \sum_{n=0}^{N} C_n T_n(\hat{z}). \tag{21}$$

The key step in the Chebyshev polynomial expansion method is to compute the integrals I_n. We evaluate the integral for every D value using the adaptive Lobatto quadrature [28] numerical integral routine 'quadl' in MATLAB to compute I_n. This ensures an accurate calculation of the integrals.

3. Convergence studies using numerical simulations

In order to demonstrate the feasibility of the above reconstruction algorithm, we first apply the method on data acquired from numerical simulations. The Fortran DDASKR routine in DASKR package [29] which is capable of solving stiff, nonlinear and nonsmooth ordinary differential equations is used to numerically simulate the dynamic approach curves of a Silicon tip on a soft elastic sample using equation (1) with the Derjaguin–Muller–Toporov (DMT) interaction model. In the DMT interaction model, van der Waals and DMT contact forces (F_{vdW}, F_{DMT}) between a sphere (tip apex) with radius R and a flat surface (sample) are assumed. For this sphere-flat surface geometry, the conservative tip sample interaction force (F_{tsc}) is defined piecewise as

$$F_{\text{tsc}}(z) = \begin{cases} -\dfrac{HR}{6z^2}, & \text{for } z > a_0 \\ -\dfrac{HR}{6a_0^2} + \dfrac{4}{3}E^*\sqrt{R}(a_0 - z)^{3/2}, & \text{for } z \leqslant a_0 \end{cases} \tag{22}$$

where H is the Hamaker constant (Joules), R the tip radius, and z the instantaneous tip–sample separation, a_0 the intermolecular distance at which contact is initiated. E^* is the effective elastic modulus of tip and sample and given by

$$\frac{1}{E^*} = \frac{1 - \nu_t^2}{E_t} + \frac{1 - \nu_s^2}{E_s}, \tag{23}$$

where ν_t, E_t, ν_s, and E_s are respectively the Poisson's ratio and the Young's modulus of the tip and sample.

For viscoelastic polymer samples, the nonconservative forces are mainly due to the Kelvin–Voigt viscoelastic contact

[1] In the experiments, the absolute value of nearest distance D is unknown. However for any nearest distance D, any change in choice of D will result in the same amount of change in the tip sample distance z in the reconstructed force distance curve. Therefore, we can assume an arbitrary nearest distance D and reconstruct the corresponding force distance curve. In the reconstructed force distance curve, the tip sample distance z only has a relative meaning.

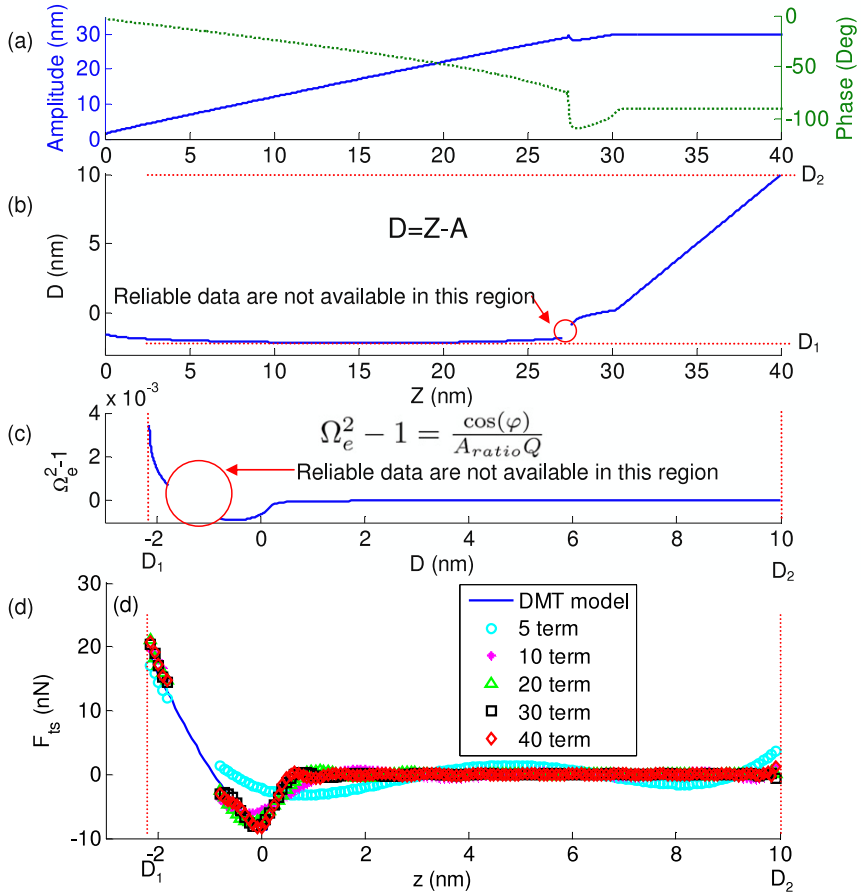

Figure 2. Numerically simulated (a) amplitude, phase and (b) nearest tip–sample distance D using the DMT interaction model versus cantilever sample gap Z, (c) frequency shift $(\Omega_e^2 - 1)$ versus nearest tip–sample distance D. D_1 and D_2 define the range of z for which the $F_{\text{tsc}}(z)$ is reconstructed, i.e. $D_1 \leqslant z \leqslant D_2$, $D_1 = -2.14$ nm, and $D_2 = 10.00$ nm. Reliable simulation data are not available in $-1.77 \leqslant z \leqslant -0.80$ nm region, (d) the reconstructed conservative tip–sample interaction forces F_{tsc} with 5 term, 10 term, 20 term, 30 term, and 40 term Chebyshev polynomial expansions are compared with the original DMT force F_{tsc} used in the numerical simulation. The RMS difference between 40 term reconstruction and original F_{tsc} is about 0.83 nN.

Table 1. Constants and properties of the MikroMasch NSC15 silicon microcantilever and the PVC (poly vinyl chloride) and HDPE (high density poly ethylene) polymer samples.

Description	Value
Bending stiffness	$k_c = 65.34$ N m^{-1}
1st natural frequency	$f_1 = 322.42$ kHz
Q factor (in air)	$Q = 980.42$
Tip radius	$R = 10$ nm
Effective elastic modulus (Si-PVC)	$E^* = 3.0$ GPa
Effective elastic modulus (Si-HDPE)	$E^* = 1.1$ GPa

damping [30]. When the tip is in contact with the sample, the nonconservative contact damping force may be represented as follows,

$$F_{\text{tsnc}}(z, \dot{z}) = \eta \dot{z} \sqrt{R(a_0 - z)}, \tag{24}$$

where, η is the sample viscosity.

For this simulation, $\Omega = 1$, $Q = 400$, $A_0 = 30$ nm, $k_c = 40$ N m^{-1}, $E^* = 1.2$ GPa, $H = 7.1 \times 10^{-20}$ J, $R = 20$ nm and $a_0 = 0.164$ nm (from García and San Paulo [31], see table 1).

The procedure to reconstruct the tip–sample interaction forces is as follows.

(1) Based on the amplitude versus distance curve (A versus Z) as shown in figure 2(a), we can generate a curve for the nearest tip–sample distance $D = Z - A$ as a function of cantilever sample gap Z as shown in figure 2(b).

(2) D_1 and D_2 define the limits of the tip–sample gap $z \in [D_1, D_2]$ for which the interaction force $F_{\text{tsc}}(z)$ is to be reconstructed. D_1 is chosen as the minimum value of D from figure 2(b), $D_1 = D_{\text{min}} = -2.14$ nm, while the choice of D_2 is somewhat open to interpretation. Generally, D_2 should be chosen in a region that interaction force F_{tsc} is nearly zero and D decreases proportionally with the decrease of cantilever sample gap Z. For the D versus Z curve in figure 2(b), for instance we could choose $D_2 = 10$ nm. A convergence study on the influence of the choice of D_2 on the reconstruction is presented in the latter part of this section.

(3) Since we have the relationship between D and Z (as shown in figure 2(b)), we can plot the frequency shift $(\Omega_e^2 - 1)$ using equation (11) as a function of the nearest tip–sample distance D as shown in figure 2(c). The

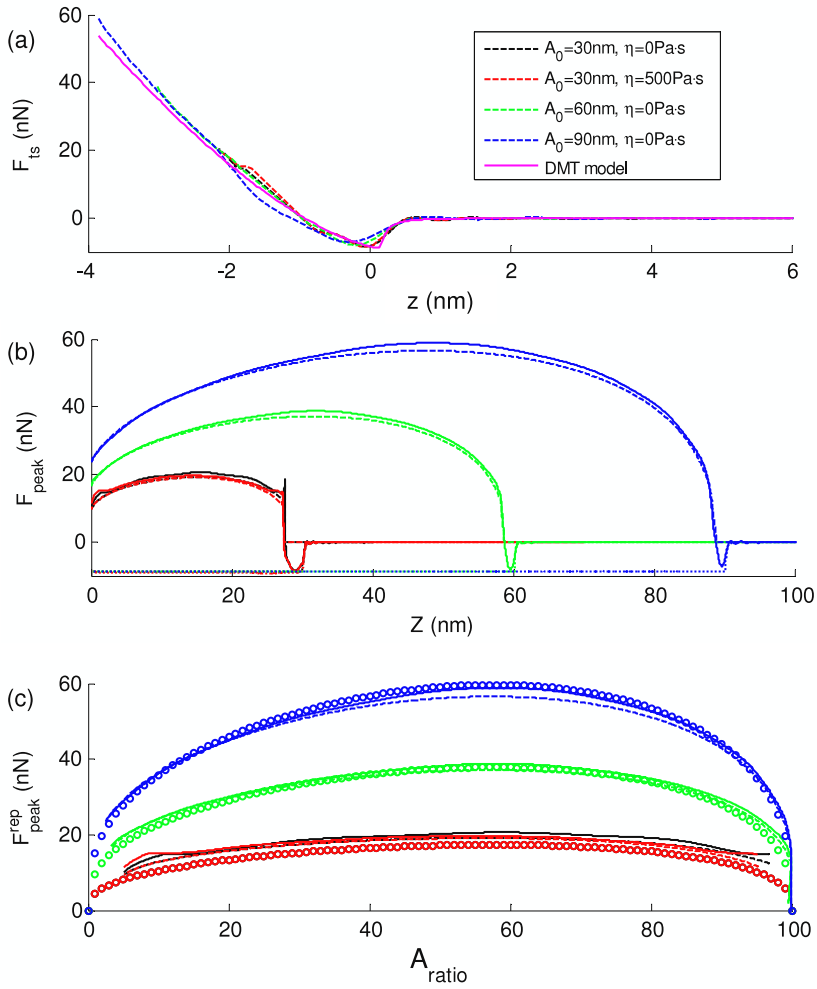

Figure 3. (a) The reconstructed conservative tip–sample interaction forces F_{tsc} (in dashed lines) are compared with the original DMT force F_{tsc} (in solid line) used in the numerical simulation as a function of distance z, (b) the reconstructed peak interaction forces F_{peak} (in solid lines) are compared with the numerically simulated peak attractive force $F^{\mathrm{att}}_{\mathrm{peak}}$ (in dotted lines) and peak repulsive forces $F^{\mathrm{rep}}_{\mathrm{peak}}$ (in dashed lines) as a function of Z gap, (c) the reconstructed peak repulsive interaction forces $F^{\mathrm{rep}}_{\mathrm{peak}}$ (in solid lines) are compared with the numerically simulated (in dashed lines) and analytically predicted (in circles) $F^{\mathrm{rep}}_{\mathrm{peak}}$ as a function of A_{ratio}. 40 term Chebyshev polynomial expansion is used for initial amplitude $A_0 = 30$ (in black), 30 (in red), 60 (in green), 90 nm (in blue) and corresponding viscosity $\eta = 0$, 500, 0, 0 Pa s.

frequency shift $\Omega_e^2 - 1$ is positive in the *net repulsive regime* and negative in the *attractive regime*. When Z decreases to -0.8 nm, the tip oscillation jumps from the attractive regime to the net repulsive regime. This transition implies that the minimum tip–sample approach D undergoes a jump from -0.80 to -1.77 nm as shown in figure 2(b). Since this range of D values is not accessible in this particular simulation, the force cannot be reconstructed for these values of tip–sample gap. However in our method it is possible to reconstruct the interaction forces once the tip is in the net repulsive regime; this is not possible using Hölscher's method [18].

(4) Then the integrals $I_n = \int_D^{D_2} T_n(\hat{z}) \frac{z-D-A}{\sqrt{A^2-(z-D-A)^2}}\,\mathrm{d}z$ are integrated numerically with the 'quadl' numerical integration routine in MATLAB. Finally, the matrix equation equation (20) can be inverted with QR decomposition method in MATLAB to solve for the Chebyshev coefficients and to reconstruct the conservative tip–sample interaction forces with equation (21).

Consider first the reconstruction of F_{tsc} from the above simulation using $D_1 = D_{\min} = -2.14$ and $D_2 = 10$ nm. The reconstructed conservative tip–sample interaction forces F_{tsc} with 5 term, 10 term, 20 term, 30 term and 40 term Chebyshev polynomial expansion are compared with the original DMT contact force F_{tsc} used in the numerical simulation in figure 2(d). Notice that because there is no reliable data for $D \in [-1.77, -0.80]$ nm, the reconstructed F_{tsc} does not converge in this region and is not shown in figure 2(d). The tendency to converge with the inclusion of more Chebyshev polynomials is obvious as shown in figure 2(d) for D outside $[-1.77, -0.80]$ nm. We find that the use of $N = 40$ reconstructs the original DMT interaction model to within 0.8 nN error (root mean squared) and the solution is deemed to be converged. Notice that in spite of the excellent convergence with $N = 40$ as shown in figure 2(d), the reconstructed force error is large near the slope discontinuity in the force model ($z \approx a_0$) as expected due to the Gibbs phenomenon.

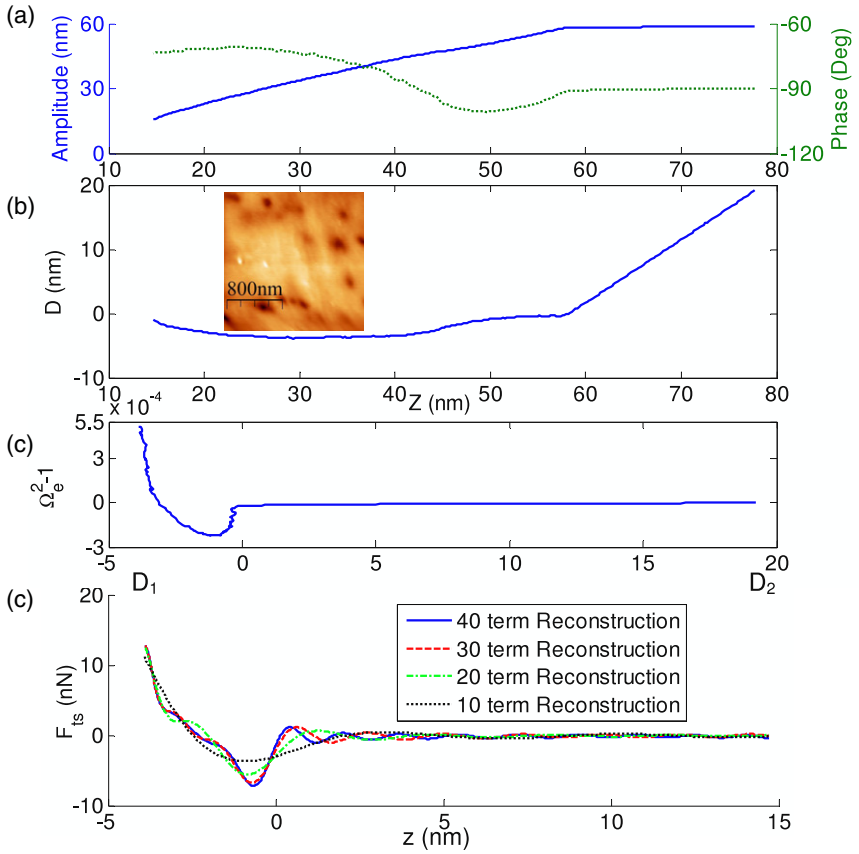

Figure 4. Experimentally measured (a) amplitude, phase and (b) nearest tip–sample distance D versus cantilever sample gap Z, (c) experimentally measured frequency shift $(\Omega_e^2 - 1)$ versus nearest tip–sample distance D on the PVC polymer sample, (d) the reconstructed conservative tip–sample interaction forces F_{tsc} with 10 term, 20 term, 30 term, and 40 term Chebyshev polynomial expansion as a function of distance z from the experimentally measured dynamic force distance curve on the PVC polymer sample. D_1 and D_2 defines the distance z domain ($D_1 \leqslant z \leqslant D_2$) for the reconstructed interaction force $F_{tsc}(z)$, $D_1 = D_{min} = -3.9$ nm and $D_2 = -5D_1 = 19.5$ nm. Initial amplitude $A_0 = 59$ nm. The inset image is the topology image of PVC sample.

In order to systematically study the influence on reconstruction error of the number of polynomial terms and choice of D_2 values, the root mean square (RMS) value of the force error is studied with increasing number of Chebyshev polynomial terms for $D_2 = 2$, 6, 8, 10, 20, 30 nm. The RMS errors decrease with an increase of terms indicating that the Chebyshev polynomial expansion converges. We also find that for this simulation, for any $D_2 \geqslant 4$ nm the convergence of the RMS error is quite good. However, in experiments, long range interaction forces could occur, and so D_2 should be chosen to ensure not only good convergence but to span the length scale over which significant interactions are expected. With this in mind, in all the reconstructions from experimental data, we will maintain $D_2 = -5D_1$.

In addition to the reconstruction of tip–sample interaction force, it is possible to use the present method to reconstruct peak interaction forces from amplitude and phase distance curves. Since the graph of D versus Z is single-valued, as shown in figure 2(b), at each Z value we know uniquely the nearest approach distance of the tip (D). If the interaction forces are primarily conservative in nature then the peak interaction force corresponds to the reconstructed interaction force evaluated at the closest approach distance. This peak value corresponds to the peak attractive force in the *attractive regime* and peak repulsive force in the *net repulsive regime*.

Finally we demonstrate that the reconstructed interaction forces are independent of the sample viscosity and initial amplitude chosen for the simulation. The amplitude and phase distance curves for two different initial amplitudes $A_0 = 60$ and 90 nm are numerically simulated to reconstruct the conservative interaction forces F_{tsc} and peak interaction forces F_{peak}. In addition, the conservative interaction force is reconstructed from a numerical simulation for $A_0 = 30$ nm but with the Kelvin–Voigt viscoelastic contact model [31] using a viscosity $\eta = 500$ Pa s. For all these cases, $D_2 = -5D_1$ and a 40 term Chebyshev polynomial expansion is implemented. As shown in figure 3(a), reconstructed conservative interaction forces F_{tsc} for $A_0 = 30$, 60, 90 nm match well with the original DMT force model. Also notice from figure 3(a) that the inclusion of sample viscosity has very little effect to the reconstruction of the conservative interaction forces F_{tsc}. This is because the nonconservative interactions only affect the effective nonlinear damping factor ζ_e and should not affect the effective nonlinear resonance frequency Ω_e.

In summary, our approach to reconstruct the conservation interactions works well even in the presence of nonconservative interactions. The reconstructed peak interaction forces

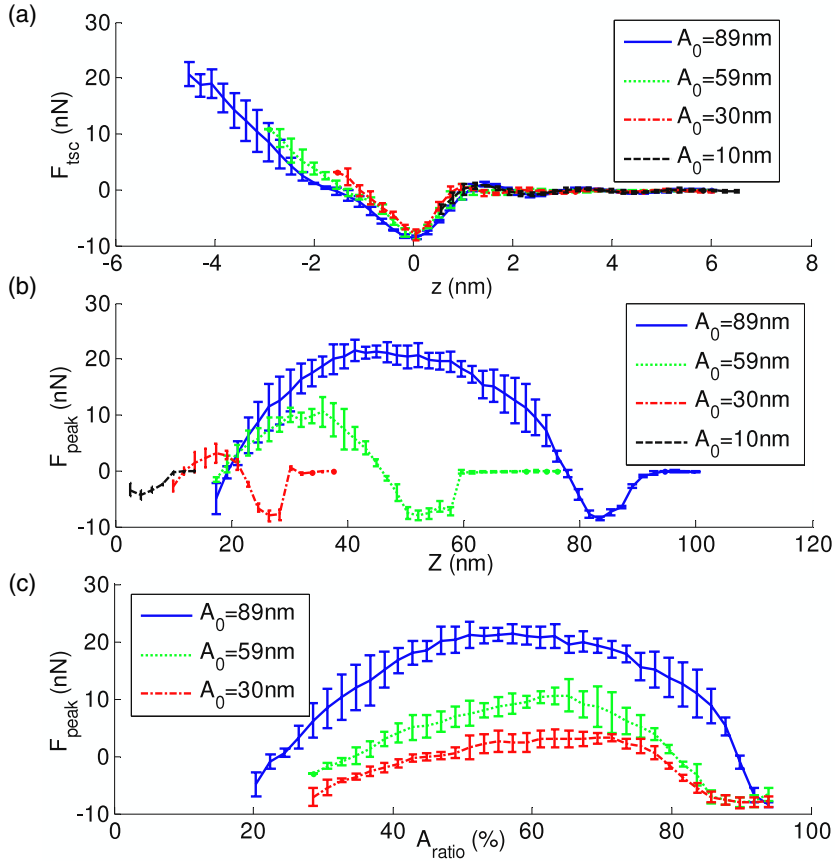

Figure 5. Error bar plot for (a) the reconstructed conservative tip–sample interaction forces F_{tsc} versus distance z, (b) the reconstructed peak interaction force F_{peak} versus Z gap, (c) the reconstructed peak interaction force F_{peak} versus A_{ratio} with 40 term Chebyshev polynomial expansion with initial amplitude $A_0 = 10$ (in dashed lines), 30 (in dashdot lines), 59 (in dotted lines), 89 nm (in solid lines). The standard deviation is computed from five experimentally measured dynamic force distance curves on the PVC polymer sample.

F_{peak} for the above simulations also are very close to the numerically simulated peak forces as shown in figure 3(b). Finally, the reconstructed peak repulsive forces match excellently with the numerical simulations and analytical predictions given in Hu and Raman [32] for all the above cases.

4. Interaction force reconstruction from experimental data

In order to test the validity of the reconstruction algorithm described above, extensive experiments have been carried out using MikroMasch NSC15 silicon microcantilevers on HDPE (high density poly ethylene) polymer and PVC (poly vinyl chloride) polymer samples. The properties of the silicon cantilever are listed in table 1. The quality factor Q is calibrated with the modal circle-fit method [33] which uses information of frequency response in the entire resonance bandwidth. The cantilever stiffness is calibrated with Sader's method [34].

The experiments are performed on a commercial Agilent Picoplus™ AFM system, together with an external Signal Recovery™ lock-in amplifier, using a MikroMasch™ UltraSharp NSC15 diving-board silicon microcantilever (properties are shown in table 1).

The experimental procedure is as follows. The amplitude and phase distance curves with four different initial amplitudes $A_0 = 10, 30, 59, 89$ nm are measured with the drive frequency equals the linear resonance frequency ($\Omega = 1$). Each set amplitude and phase distance curve is repeated at least five times.

First consider the reconstruction from data acquired on the PVC sample using $A_0 = 59$ nm. The amplitude and phase versus distance curves for $A_0 = 59$ nm are shown in figure 4(a). Then the closest tip sample distance D versus Z curve is computed based on the amplitude distance curve as shown in figure 4(b). Notice that unlike in the simulations, the Z values in experiments are not absolute but rather relative quantities. Thus the experimentalist has to define or choose the location of $Z = 0$. Fortunately, the reconstruction method is insensitive to the choice of $Z = 0$ because this choice only causes a linear shift in the z axis of the reconstructed force plot. Then the frequency shift $(\Omega_e^2 - 1)$ is computed using equation (10) as a function of the nearest tip–sample distance D as shown in figure 4(c). The frequency shift $\Omega_e^2 - 1$ is positive in the *net repulsive regime* and negative in *net attractive regime*. The experimentally measured Frequency shift $\Omega_e^2 - 1$ is relatively smooth compared to the numerical simulations. Then the conservative interaction force F_{tsc} is reconstructed using the Chebyshev expansion method with

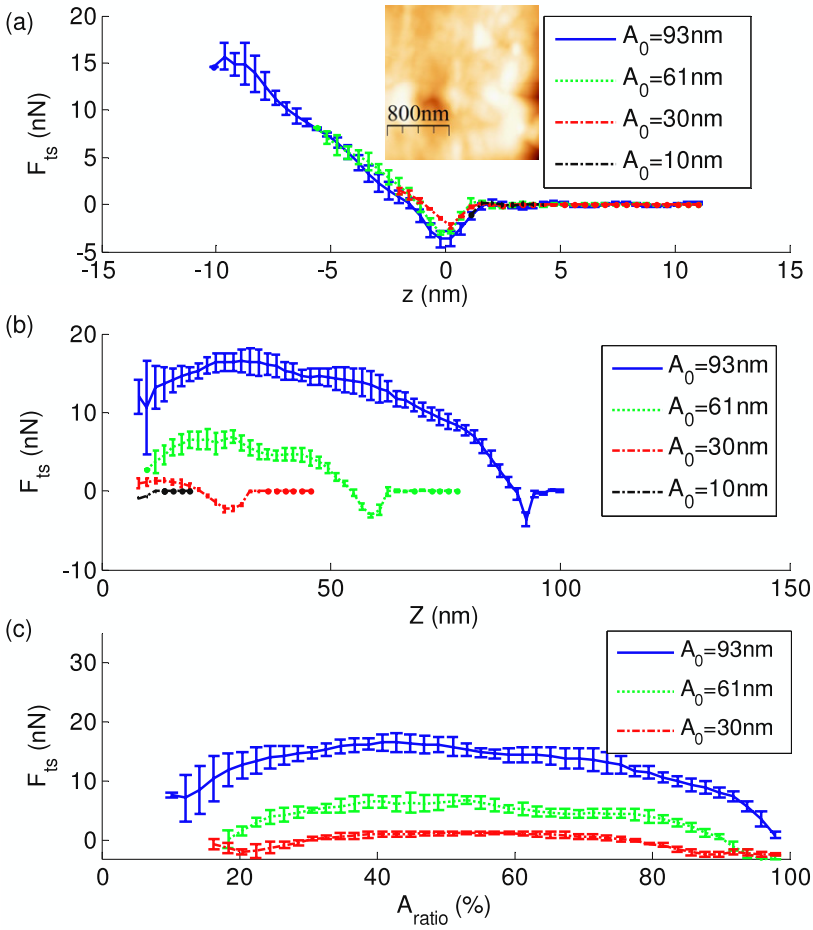

Figure 6. Error bar plot for (a) the reconstructed conservative tip–sample interaction forces F_{tsc} versus distance z, (b) the reconstructed peak interaction force F_{peak} versus Z gap, (c) the reconstructed peak interaction force F_{peak} versus A_{ratio} with 40 term Chebyshev polynomial expansion with initial amplitude $A_0 = 10$ (in dashed lines), 30 (in dash–dot lines), 61 (in dotted lines), 93 nm (in solid lines). The standard deviation is computed from five experimentally measured dynamic force distance curves on the HDPE polymer sample. The inset image is the topology image of HDPE sample.

$D_1 = D_{\text{min}} = -3.9$ nm and $D_2 = -5D_1 = 19.5$ nm. The reconstructed F_{tsc} with 10 term, 20 term, 30 term and 40 term expansions are shown in figure 4(d) indicating that a 40 term expansion is sufficient for the purpose.

To demonstrate the consistence of the Chebyshev expansion method, the reconstructed F_{tsc} with $A_0 = 10$, 30, 59, 89 nm, with five different trials each are plotted in figure 5(a). The standard deviation (error bar) is computed from five different trials. From figure 5(a) it is clear that the reconstructed F_{tsc} for different initial amplitudes collapse on top of each other thus demonstrating the robustness of this method. The peak interaction forces are also reconstructed as a function of Z and A_{ratio} from the experimental data in figures 5(b) and (c).

Next we consider the results based on experiments performed on a HDPE sample ($E^* \approx 1.1$ GPa) which is softer than the PVC sample ($E^* \approx 3.0$ GPa). As shown in figure 6(a), the reconstructed F_{tsc} of the HDPE sample is smaller (both attractive and repulsive) than that of the PVC sample while the indentation is about twice of the PVC sample.

From the reconstructions performed on PVC and HDPE it is clear that (a) smaller A_0 values lead to smaller peak forces, (b) smaller E^* leads to smaller peak forces, and (c) peak forces reach their maxima at $A_{\text{ratio}} \approx 50$–$60\%$. All these general trends agree with the analytical predictions given in [31]. The experimental analysis clearly shows that the proposed method is robust and leads to repeatable reconstruction and measurement of tip–sample interaction forces. From the reconstructed interaction forces shown in figures 5 and 6, there are significant attractive forces and adhesion forces for all the polymer samples tested. Moreover a simple Herzian contact model may not be accurate to describe the repulsive interactions in these polymer samples. PVC samples were found to have relatively large adhesion forces (around 8 nN) compared to the HDPE samples (around 4 nN).

5. Summary and conclusions

The integral theory and reconstruction algorithm for AM-AFM proposed in this work offers several advantages.

(1) The reconstruction of conservation interactions and peak interaction forces is relatively robust and can be implemented with the presence of nonconservative

interactions and the instabilities due to the jump from attractive to repulsive regime.

(2) The theoretical approach is not limited to the large amplitude or short range force assumption.

(3) This method only requires the experimentally measured amplitude and phase distance curves in AM-AFM that are routinely accessible in all commercial AFM systems with commercially available cantilevers. Therefore it can be easily implemented compared to other methods requiring access to the real time series data and its detailed analysis, or a significant modification of the type of microcantilever used for AFM.

(4) Finally the proposed method is model independent, thus opening the door to many different interaction measurements including chemical, electrostatic, and magnetic forces.

In spite of the above advantages, the reconstruction error is expected to be rather high in the net repulsive range for harder samples because the indentation $D = Z - A$ is very small. In such a situations unless A is measured very accurately, the reconstructed indentations and forces can be erroneous. Ultimately though, the use of AM-AFM for the reconstruction of *conservative* interactions cannot be as accurate as FM-AFM based methods because shifts in frequency can be detected much more sensitively (parts per million) compared to changes in amplitude (parts per thousand). However given the popularity of AM-AFM among AFM users, the theoretical approach outlined here will prove extremely useful to extract tip–sample interactions in AM-AFM.

In summary, in this paper, a theory and an algorithm for the reconstruction of tip–sample interaction forces in AM-AFM are developed by deriving and solving the underlying integral equation with Chebyshev polynomial expansion method. The peak interaction forces are also estimated with the reconstructed interaction forces. The feasibility of the approach and detailed convergence studies are performed using numerically simulated data. Experimentally measured amplitude and phase distance curves on polymer samples are used to reconstruct the conservative interaction forces and the peak interaction forces. This approach opens the door for quantitative interaction forces measurements and nanoscale dynamic material analysis (Nano DMA) in AM-AFM for most AFM experimentalists. Ultimately one can imagine that this algorithm will allow the AFM user to finally 'see' the unseeable imaging forces exerted on the sample in tapping mode AFM.

Acknowledgments

Financial support for this research provided by the National Science foundation through grant CMMI-0700289 is gratefully acknowledged. We also thank Professor R Reifenberger (Physics, Purdue) for valuable discussions.

Appendix. Fourier coefficients of the interaction force

Noticing that instantaneous gap and its rate are given by $z(\tau) = Z + x(\tau) = Z + A\cos(\theta)$, and $\dot{z}(\tau) = -A\sin(\theta)$, we therefore have $z = Z \pm \sqrt{1-\dot{z}^2}$. Using this relation, we have

$$
\begin{aligned}
F_{\mathrm{ts\,cos}} &= \frac{1}{\pi}\int_0^{2\pi} [F_{\mathrm{tsc}}(z) + F_{\mathrm{tsnc}}(z,\dot{z})]\cos(\theta)\,\mathrm{d}\theta \\
&= \frac{1}{\pi}\int_0^{2\pi} \bar{F}_{\mathrm{tsc}}[Z + A\cos(\theta)]\cos(\theta)\,\mathrm{d}\theta \\
&\quad + \frac{1}{\pi}\Bigg[\int_0^{\pi/2} F_{\mathrm{tsnc}}(z,\dot{z})\cos(\theta)\,\mathrm{d}\theta \\
&\quad + \int_{\pi/2}^{\pi} F_{\mathrm{tsnc}}(z,\dot{z})\cos(\theta)\,\mathrm{d}\theta \\
&\quad + \int_{\pi}^{3\pi/2} F_{\mathrm{tsnc}}(z,\dot{z})\cos(\theta)\,\mathrm{d}\theta \\
&\quad + \int_{3\pi/2}^{2\pi} F_{\mathrm{tsnc}}(z,\dot{z})\cos(\theta)\,\mathrm{d}\theta\Bigg] \\
&= \frac{1}{\pi}\int_0^{2\pi} \bar{F}_{\mathrm{tsc}}[Z + A\cos(\theta)]\cos(\theta)\,\mathrm{d}\theta \\
&\quad - \frac{1}{\pi A}\Bigg[\int_0^{-1} F_{\mathrm{tsnc}}(Z+\sqrt{1-\dot{z}^2},\dot{z})\,\mathrm{d}\dot{z} \\
&\quad + \int_{-1}^{0} F_{\mathrm{tsnc}}(Z-\sqrt{1-\dot{z}^2},\dot{z})\,\mathrm{d}\dot{z} \\
&\quad + \int_{0}^{1} F_{\mathrm{tsnc}}(Z-\sqrt{1-\dot{z}^2},\dot{z})\,\mathrm{d}\dot{z} \\
&\quad + \int_{1}^{0} F_{\mathrm{tsnc}}(Z+\sqrt{1-\dot{z}^2},\dot{z})\,\mathrm{d}\dot{z}\Bigg] \\
&= \frac{1}{\pi}\int_0^{2\pi} \bar{F}_{\mathrm{tsc}}[Z + A\cos(\theta)]\cos(\theta)\,\mathrm{d}\theta \\
&\quad - \frac{1}{\pi A}\int_0^{-1} [F_{\mathrm{tsnc}}(Z+\sqrt{1-\dot{z}^2},\dot{z}) \\
&\quad + F_{\mathrm{tsnc}}(Z+\sqrt{1-\dot{z}^2},-\dot{z})]\,\mathrm{d}\dot{z} \\
&\quad - \frac{1}{\pi A}\int_{-1}^{0} [F_{\mathrm{tsnc}}(Z-\sqrt{1-\dot{z}^2},\dot{z}) \\
&\quad + F_{\mathrm{tsnc}}(Z-\sqrt{1-\dot{z}^2},-\dot{z})]\,\mathrm{d}\dot{z} \\
&= \frac{1}{\pi}\int_0^{2\pi} \bar{F}_{\mathrm{tsc}}[Z + A\cos(\theta)]\cos(\theta)\,\mathrm{d}\theta. \qquad \text{(A.1)}
\end{aligned}
$$

Thus the assumption that the nonconservative forces are antisymmetric with respect to tip velocity, $F_{\mathrm{tsnc}}(z,\dot{z}) = -F_{\mathrm{tsnc}}(z,-\dot{z})$, leads to

$$
F_{\mathrm{ts\,cos}} = \frac{1}{\pi}\int_0^{2\pi} \bar{F}_{\mathrm{tsc}}[Z + A\cos(\theta)]\cos(\theta)\,\mathrm{d}\theta. \qquad \text{(A.2)}
$$

Similarly, we have

$$
\begin{aligned}
F_{\mathrm{ts\,sin}} &= \frac{1}{\pi}\int_0^{2\pi} [F_{\mathrm{tsc}}(z) + F_{\mathrm{tsnc}}(z,\dot{z})]\sin(\theta)\,\mathrm{d}\theta \\
&= -\frac{1}{\pi A}\Bigg[\int_{Z+A}^{Z-A} F_{\mathrm{tsc}}(z)\,\mathrm{d}z + \int_{Z-A}^{Z+A} F_{\mathrm{tsc}}(z)\,\mathrm{d}z\Bigg]
\end{aligned}
$$

$$+\frac{1}{\pi}\int_0^{2\pi}\bar{F}_{\mathrm{tsnc}}[Z+A\cos(\theta),-A\sin(\theta)]\sin(\theta)\,\mathrm{d}\theta$$
$$=\frac{1}{\pi}\int_0^{2\pi}\bar{F}_{\mathrm{tsnc}}[Z+A\cos(\theta),-A\sin(\theta)]\sin(\theta)\,\mathrm{d}\theta. \quad (A.3)$$

References

[1] Sugimoto Y, Pou P, Abe1 M, Jelinek P, Pérez R, Morita S and Custance O 2007 *Nature* **446** 65
[2] Giessibl F J 1997 *Phys. Rev.* B **56** 16010
[3] Magonov S N, Elings V and Papkov V S 1997 *Polymer* **38** 297
[4] Butt H J, Cappella B and Kappl M 2005 *Surf. Sci. Rep.* **59** 1–152
[5] Hölscher H, Schwarz U D, Zwörner O and Wiesendanger R 1998 *Phys. Rev.* B **57** 2477–81
[6] Albrecht T R, Grtitter P, Horne D and Rugar D 1991 *J. Appl. Phys.* **69** 15
[7] Giessibl F J 2003 *Rev. Mod. Phys.* **75** 949
[8] Dürig U 1999 *Appl. Phys. Lett.* **75** 433
[9] Dürig U 2000 *Appl. Phys. Lett.* **76** 1203
[10] Gorenflo R and Vessella S 1991 *Abel Integral Equations: Analysis and Applications* (Berlin: Springer)
[11] Langkat S M, Hölscher H, Schwarz A and Wiesendanger R 2003 *Surf. Sci.* **527** 12
[12] Sugimoto Y, Pou P, Abe1 M, Jelinek P, Pérez R, Morita1 S and Custance O 2007 *Nature* **446** 65
[13] Hölscher H, Langkat S M, Schwarz A and Wiesendanger R 2002 *Appl. Phys. Lett.* **81** 4428
[14] Langkat S M, Hölscher H, Schwarz A and Wiesendanger R 2003 *Surf. Sci.* **527** 12
[15] Sader J E and Jarvis S P 2004 *Appl. Phys. Lett.* **84** 1801
[16] Sader J E, Uchihashi T, Higgins M J, Farrell A, Nakayama Y and Jarvis S P 2005 *Nanotechnology* **16** S94
[17] Dürig U 1999 *Appl. Phys. Lett.* **75** 433
[18] Hölscher H 2006 *Appl. Phys. Lett.* **89** 123109
[19] Sugawara Y, Kobayashi N, Kawakami M, Li Y J, Naitoh Y and Kageshima M 2007 *Appl. Phys. Lett.* **90** 194104
[20] Hölscher H 2008 *J. Appl. Phys.* **103** 064317
[21] Lee M and Jhe W 2006 *Phy. Rev. Lett.* **97** 036104
[22] Lee S I, Howell S W, Raman A and Reifenberger R 2002 *Phys. Rev.* B **66** 115409
[23] Melcher J, Hu S and Raman A 2007 *Appl. Phys. Lett.* **91** 053101
[24] Nayfeh A H and Mook D T 1979 *Nonlinear Oscillations* (New York: Wiley)
[25] Crittenden S, Raman A and Reifenberger R 2005 *Phys. Rev.* B **72** 235422
[26] Boyd J P 1999 *Chebyshev and Fourier Spectral Methods* 2nd edn (New York: Dover) pp 11–2
[27] Piessens R 2000 *J. Comput. Appl. Math.* **121** 113–24
[28] Gander W and Gautschi W 2000 *Behav. Inform. Technol.* **40** 84–101
[29] Ascher U M and Petzold L R 1999 *Computer Methods For Ordinary Differential Equations And Differential-Algebraic Equations* (Philadelphia, PA: SIAM)
[30] Garcia R, Gomez C J, Martinez N F, Patil S, Dietz C and Magerle R 2006 *Phys. Rev. Lett.* **97** 016103
[31] García R and San Paulo A 1999 *Phys. Rev.* B **60** 4961
[32] Hu S and Raman A 2007 *Appl. Phys. Lett.* **91** 123106
[33] Ewins D J 2000 *Modal Tesing: Theory, Practice and Application* 2nd edn (Baldock: Research Studies Press)
[34] Sader J E, Chon J W M and Mulvaney P 1999 *Rev. Sci. Instrum.* **70** 3967–9